Available online at www.sciencedirect.com
SCIENCE DIRECT®
Physics Letters B 636 (2006) 235–247
PHYSICS LETTERS B
www.elsevier.com/locate/physletb

Microscopic calculations of signals of double beta decay in a ^{76}Ge detector and first application to the Heidelberg–Moscow experiment

H.V. Klapdor-Kleingrothaus [*,1], I.V. Krivosheina [2], V. Mironov [3], I.V. Titkova [3]

Max-Planck-Institut für Kernphysik, PO 10 39 80, D-69029 Heidelberg, Germany

Received 17 November 2005; received in revised form 15 February 2006; accepted 19 March 2006

Available online 30 March 2006

Editor: V. Metag

Abstract

The identification of signals of neutrinoless double beta decay is a question of extreme interest. Starting from the Monte Carlo calculated time history and spatial energy distribution of neutrinoless double beta events, for the first time the expected *pulse shapes* to be observed in a big ^{76}Ge detector have been calculated '*microscopically*', by using the Poisson Superfish code for determination of the field distribution in the detector. It is shown, that for the majority of $0\nu\beta\beta$ events it is not possible to differentiate between the contributions of different particle physics parameters entering into the $0\nu\beta\beta$ decay process—in the mass mechanism the effective neutrino mass and the right-handed weak current parameters $\langle\lambda\rangle$, $\langle\eta\rangle$. It is shown, that on the other hand it is possible in a ^{76}Ge double beta decay experiment to reject a background of larger sizes (high multiplicity) gamma events by selecting low size (low multiplicity) events. First application of the theoretical $\beta\beta$ pulses to events from the line observed at $Q_{\beta\beta}$ [H.V. Klapdor-Kleingrothaus, I.V. Krivosheina, A. Dietz, et al., Phys. Lett. B 586 (2004) 198; H.V. Klapdor-Kleingrothaus, A. Dietz, I.V. Krivosheina, et al., Nucl. Instrum. Methods A 522 (2004) 371] shows very good agreement. It is shown further, and confirmed by measurements with a collimated source, that a rather good radial position determination of $\beta\beta$ events in the detector is possible. By the same type of calculation it is shown that use of the pulse shapes of the 1592 keV double escape line of the 2614 keV γ-transition from ^{228}Th for calibrating a neuronal net for search of events of neutrinoless double beta decay can be helpful.

PACS: 14.60.Pq; 23.40.-s; 29.40.-n; 95.55.Vj

Keywords: Neutrino mass and mixing; Majorana neutrino; Beta-decay; Double beta decay; Heidelberg–Moscow experiment; High purity Ge detectors

1. Introduction

The identification of signals of neutrinoless double beta decay in a ^{76}Ge detector is a question of extraordinary importance. The shapes and sizes of *tracks* of events of $0\nu\beta\beta$ decay in a germanium detector depend in principle on particle physics and nuclear physics parameters such as neutrino mass, right-handed current parameters, etc., and nuclear matrix elements. This dependence has been investigated theoretically recently [1,2]. In this Letter we investigate, starting from the tracks calculated by a Monte Carlo procedure in [1,2], the shapes of the corresponding electrical *pulses* to be expected in the detector, which depend additionally on the location of the individual event in the detector. We further investigate pulse shapes of the 1592 keV double escape line of the 2614 keV gamma line from ^{228}Th and its potential to be used for 'calibration' of the pulse shapes in a detector in search for $0\nu\beta\beta$ events. We show that the measured pulse shapes allow to reduce the background of larger sizes gamma events, and allow further a rather good radial localization of measured $\beta\beta$ events in the detector.

* Corresponding author. Tel.: +49 06221 516 262; fax: +49 06221 516 540.
E-mail address: h.klapdor@mpi-hd.mpg.de (H.V. Klapdor-Kleingrothaus).
URL: http://www.mpi-hd.mpg.de.non_acc/.
[1] Spokesman of Heidelberg–Moscow and GENIUS-TF Collaboration.
[2] On leave from Radiophysical-Research Institute, Nishnii-Novgorod, Russia.
[3] On leave from JINR, Dubna, Russia.

0370-2693/$ – see front matter
doi:10.1016/j.physletb.2006.03.048

2. Tracks and sizes of double beta and gamma events in the Ge detector

For the calculation of the tracks of $0\nu\beta\beta$ events and their resulting electrical pulse shapes in a Ge detector, three cases had been considered in our recent Monte Carlo calculations [1,2], representing the main features of the calculated angular correlations (see Figs. 3, 4 from [1] and Figs. 3–5, 7–9, 11 from [2]), between the emitted electrons for dominating terms of effective neutrino mass or right-handed weak current parameters η and λ (see [32–37] for the basic physics).

(1) Two electrons with energy 1020 keV each were started at a given point in the detector with relative angle of 180° (only the neutrino mass term considered).
(2) The directions of the electrons were the *same* and the energy distribution $0.15T$ for one electron and $0.85T$ for the other (only $\langle\lambda\rangle$ term). Here T is the total emitted energy ($= Q_{\beta\beta}$).
(3) The electrons were assumed to be emitted to the same direction with half of the total kinetic energy each (only $\langle\eta\rangle$ term).

The time history of the trajectories of electrons, positrons and gammas produced by a $\beta\beta$ (or γ) event in the detector is followed taking into account energy deposition by photoabsorption, Compton scattering, pair production and bremsstrahlung, using the code GEANT4 [31] as electron–gamma transport simulation code. Here for the $\beta\beta$ decay the two electrons were started at a defined point in the detector, the energy and the angle between their momenta were defined according to the calculated spectral-angular distributions [1,2] as given in points (1)–(3) above. The values of the energy depositions and coordinates of each interaction in the decay processes were written in data files.

Some examples of calculated tracks of $0\nu\beta\beta$ events in the germanium detector are shown in [1,2] and presented in Fig. 1. The places of the energy depositions in germanium are indicated as circles. The sizes and colours of these circles indicate the amount of energy released at these points. Green straight lines denote γ-events (bremsstrahlung) in case of $\beta\beta$ decay, annihilation gammas in case of absorption of a γ by pair creation, all other events are electron(positron)–electron scattering.

Considering the sum energy of the electrons, most events (94%) lie in the sharp main peak at $Q_{\beta\beta}$ (2039 keV [6–9] see [1]). Events with bremsstrahlung emission correspond to only 2.23% of the started events.

Fig. 1 shows also an example of a photon event in the detector corresponding to a 2614 keV photon from ^{228}Th. In the spectrum seen in the detector (according to the Monte Carlo simulation) from the 2614 keV γ-transition, besides the full energy (FE) peak at 2614 keV the single escape (SE) and double escape (DE) peaks occur, resulting from absorption of the 2614 keV γ-quant by e^+e^- pair creation and subsequent annihilation of the positron with an electron and emission of two 511 keV γ-quanta, of which one (SE) or both (DE) escape from the detector (see, e.g., [2,4,21]). The event shown in Fig. 1 corresponds just to such type of event, which is of special interest in this investigation, since it is rather similar to a $\beta\beta$ event.

The $0\nu\beta\beta$ examples shown in Fig. 1 are idealized cases: (1) only one of the terms $\langle m\rangle$, $\langle\lambda\rangle$, $\langle\eta\rangle$ contributes; (2) only examples for the most probable of the many possibilities of angular correlations allowed are shown.

The sizes of individual events such as shown in Fig. 1 were defined in two ways. The *linear size* is the maximum distance between places of energy depositions without paying attention to the values of latter:

$$R_l = \max\left[\sqrt{(x_i - x_j)^2 + (y_i - y_j)^2 + (z_i - z_j)^2}\right]. \tag{1}$$

In the *weighted* size the values of energy deposited in each point were taken into account:

$$R_w = \frac{\sum_{i,j} \epsilon_i \epsilon_j \sqrt{(x_i - x_j)^2 + (y_i - y_j)^2 + (z_i - z_j)^2}}{\epsilon^2{}_{\text{total}}}, \tag{2}$$

where ϵ_{total} is the full energy, deposited for this event in the detector. While naturally in the first case in a range of diameter R_l, 100% of the released energy is contained, in the 'weighted' case a volume with diameter R_w contains typically about 60% of the total released energy.

In the analysis of sizes of events the cases (1)–(3) above were considered for $0\nu\beta\beta$ decay, i.e., cases of dominating m, λ, η. It has been found [1,2] that the overwhelming part of $0\nu\beta\beta$ events lies within a size of ~ 2 (~ 0.3) mm for the linear (weighted) case. The intensities have a maximum of the linear (weighted) sizes of ~ 1 (~ 0.25) mm (see Fig. 2 and Figs. 17–19 in [2]).

The situation with the 1592 keV double escape (DE) gamma events is quite similar (Fig. 2). Since the double escape events are also sharply localized in the detector their size is very similar to the $0\nu\beta\beta$ events, but systematically slightly *smaller*. The overwhelming part of the double escape events is lying within a distance of 1.3 (0.4) mm, with the maximum of the distribution lying for linear (weighted) sizes at ~ 0.7 (~ 0.2) mm. The distribution of sizes for 'normal' γ-lines (their full energy peaks) is quite different from those of $0\nu\beta\beta$ (and γ-double escape lines) (see Fig. 2). The sizes are usually much larger. For a more detailed discussion see [1,2].

3. 'Microscopic' calculations of pulse shapes

3.1. The calculation method

A calculation of pulses in a Ge detector corresponding to Monte Carlo calculated $\beta\beta$ events (tracks) is done here for the first time. We perform this for the big high-purity ^{76}Ge detectors of the Heidelberg–Moscow experiment. A standard procedure is used to calculate the pulses. The charges (electrons and holes) produced in the $\beta\beta$ or γ-events (see Fig. 1) migrate in the Ge crystal according to the applied electric field, which depends on the geometry of the detector (in our case semi-coaxial p-type with dimensions of the enriched detectors of the Heidelberg–Moscow $\beta\beta$ experiment, see Table 2) the applied voltage, the intrinsic space-charge density ρ and the carrier mobility μ.

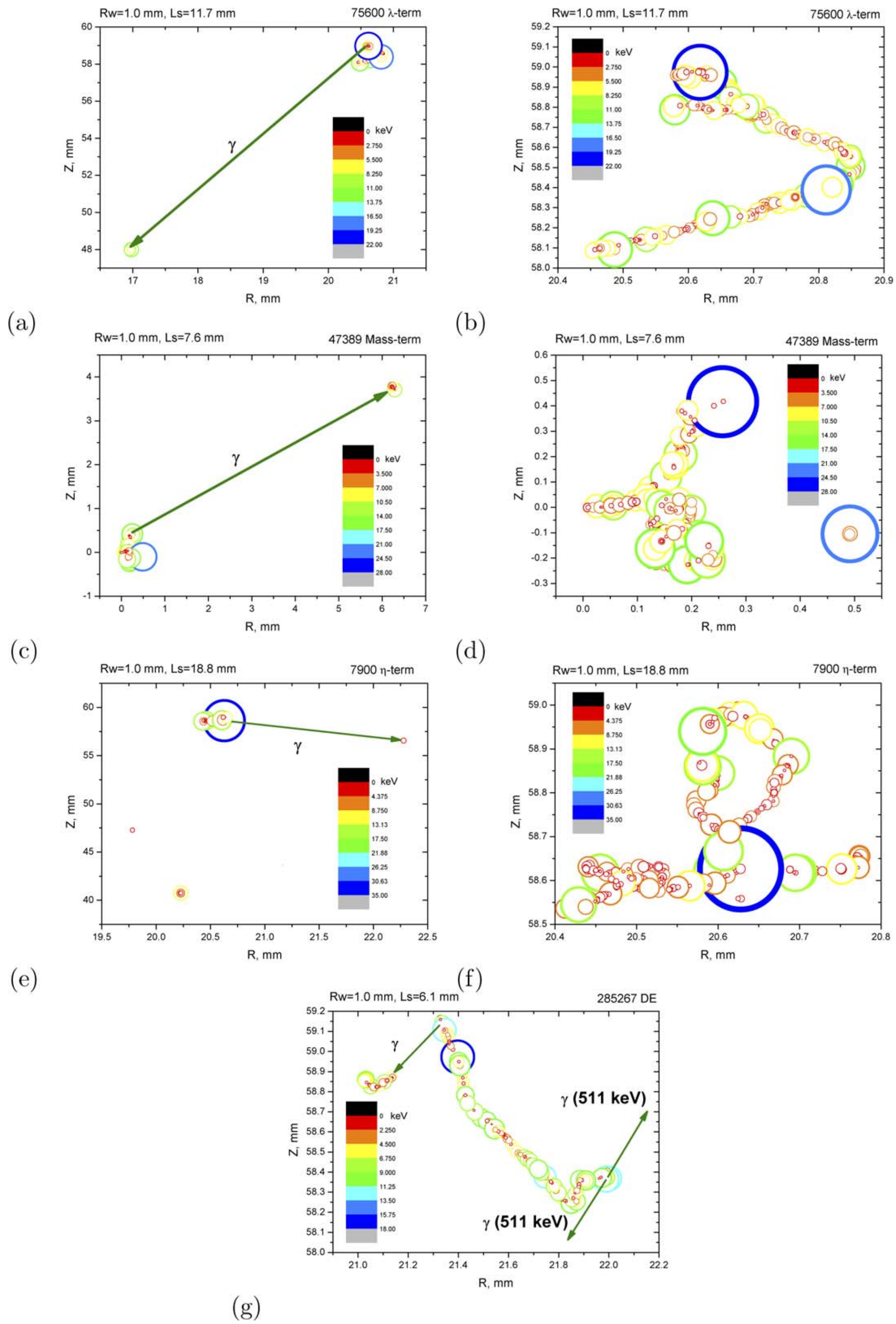

Fig. 1. Some typical calculated events for $0\nu\beta\beta$ decay for cases of dominating: $\langle\lambda\rangle$ (a), (b) ((a)—full event, (b)—zoom of this event); (c) and (d)—$\langle m\rangle$, (e), (f) for $\langle\eta\rangle$ term in the $0\nu\beta\beta$ process; (g): calculated photon event (the energy of the initial photon is 2614 keV) for the double escape case (leading to a line in the detector at 1592 keV).

The calculations of pulses consist of tracing the movement of positive and negative electric charges inside the crystal starting from the different positions inside the crystal in such a way as to calculate the detected current. The electric field has been calculated by the Poisson Superfish code [20] (real and weighting fields, see below) over the detector volume (with radius R and height Z) with a grid size of 64×64. The field in a given point between the grid points then is found by a spline inter-

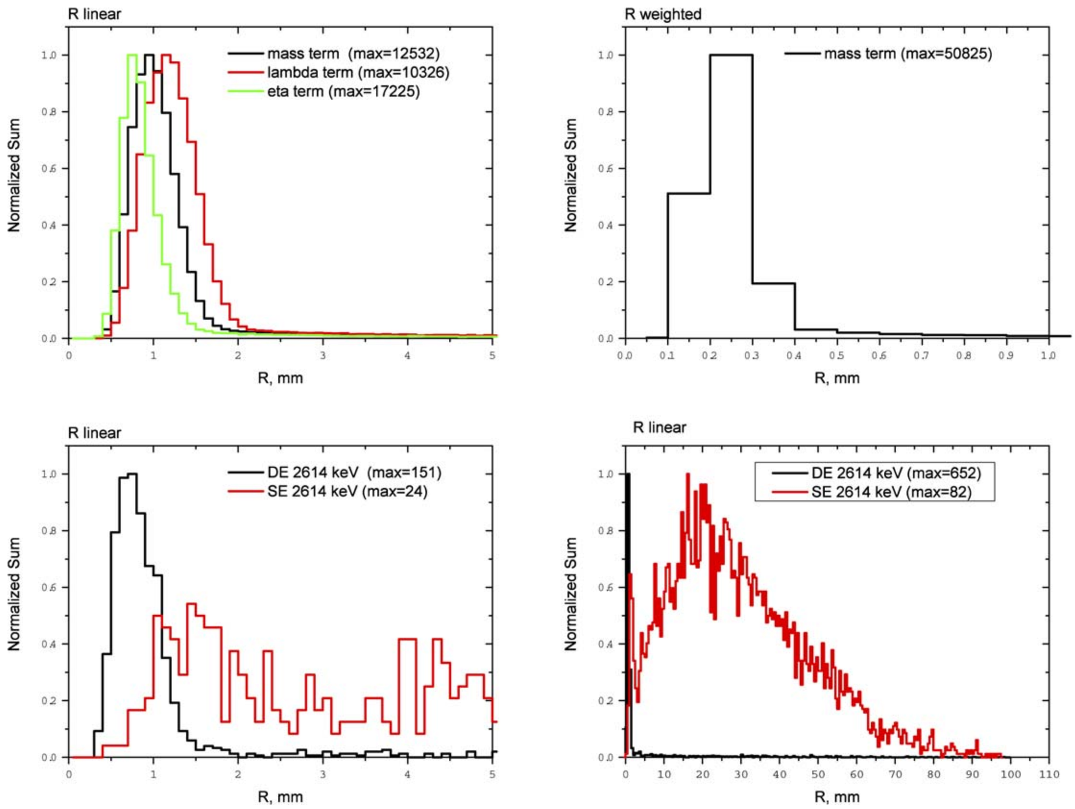

Fig. 2. Distribution of sizes (linear and weighted) in a Ge detector of various types of $0\nu\beta\beta$ events, and of the γ-line at 2614 keV, and its single and double escape lines at 2103 keV and 1592 keV, respectively, according to Monte Carlo simulations of these events taking into account the angular correlations between the emitted electrons in $0\nu\beta\beta$ decay (from [2]). The ordinate axis is normalized to the maximum of the distribution in each case.

polation of the Poisson Superfish output data. In generating the charge carrier trajectories a time interval of 4×10^{-11} s is used, which is small enough to avoid any discontinuities of the drift velocities. The charge equilibrium velocity is assumed to be reached instantaneously and lateral diffusion of charge carriers (perpendicular to the electric field) has been neglected, as well as plasma effects, trapping and detrapping [21].

The contributions to the total current $i(t) = i_e(t) + i_h(t)$ can be calculated according to the equation

$$i_{e(h)}(t) = -q_{e(h)} \vec{E}_w \vec{V}_{e(h)}(t), \tag{3}$$

where $i_{e(h)}$ are the current due to the electron and hole motion, $q_{e(h)}$ is the electric charge of a carrier, $\vec{E}_w$ is the so-called weighting field [26], and $\vec{V}_{e(h)}$ is the carrier drift velocity that is directed along the real electric field vector inside the crystal. According to the Shockley–Ramo theorem [26–28] the weighting electric field is calculated by setting the impurity space charge in the crystal to zero and by putting a unity voltage to the signal electrode with keeping all other electrodes at a zero voltage [22,29] (see Fig. 3). We adopted the following empirical dependence of the carrier drift velocity of electrons on the electric field inside the crystal [22]

$$V_e = \frac{\mu_0 E}{(1 + (E/E_0)^{\beta})^{1/\beta}} - \mu_n E, \tag{4}$$

where the fit parameters are different for different directions with respect to the crystal orientation (see Table 1). The elec-

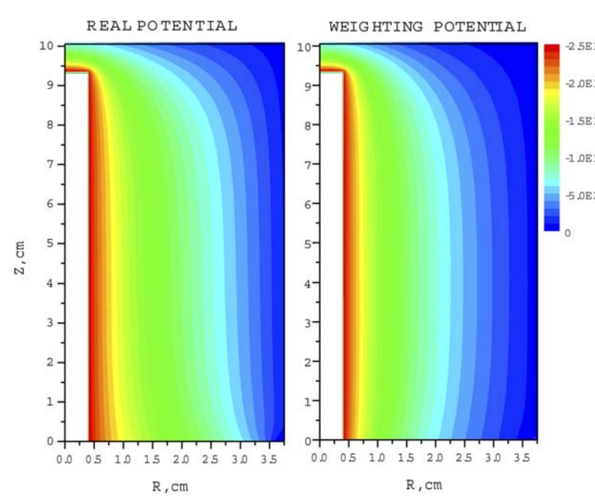

Fig. 3. Electric field as calculated by the Poisson Superfish code [20] for the detector ANG5 of the Heidelberg–Moscow experiment in Gran Sasso (real (left) and weighting (right) fields). The chosen ionized impurity density is 1.875×10^9 cm^{-3} (included in the left, but set to zero in the right part). Operational voltage is 2500 V.

tron mobility at the given point is then dependent on the angle between the carrier velocity and crystallographic axes. It was calculated by linear extrapolation between mobilities in the $\langle 100 \rangle$ and $\langle 111 \rangle$ as a function of the angular directions, assuming the $\langle 100 \rangle$ axis to be parallel to the crystal symmetry axis. Concerning the hole mobility as a function of the electric field, we used a fit at the experimentally measured dependence of the hole-drift velocities as a function of electric field in the ⟨100⟩ direction (from [19]) with a generalized-hyperbola:

$$V_h = A - \frac{B}{(1 + C \cdot E)^{1/D}}, \tag{5}$$

where the fit parameters are: $A = B = 1.22 \times 10^7$ cm/s, $C = 6.15 \times 10^{-3}$ cm/V, $D = 1.514$.

The signal electrode (bore of the crystal) was biased negatively and the outer boundary of the crystal supposed to be at the ground potential everywhere except the bottom surface. In the real crystals there is placed a grounded copper plate below the bottom surface. We set this plate negatively biased when calculating the real electric field, and grounded when calculating the weighting field. *The ionized impurity density* (space charge density) given by the manufacturers (see Table 2) was approximated by a constant distribution (see Section 3.3).

As example the calculated electric field distribution inside the crystal is shown for the detector No. 5 of the Heidelberg–Moscow experiment in Fig. 3. Both real and weighting fields are shown. The output of the field calculations was written into a table, which was read in the following by the pulse-shape calculation code written in Compaq Visual Fortran 6.5 language, with the use of IMSL Fortran libraries [30].

After finishing the calculations for *one* initial position, the calculated electron and hole currents were summed and convoluted in order to take into account the shaping in the preamplifier/amplifier electronic circuits. For this, we used the convolution function as suggested in [22]:

$$g(t) = \frac{1}{T_d - T_r\sqrt{\pi}/(2\sqrt{1.3})} \times \left[\exp\left(-\frac{t}{T_d}\right) - \exp\left(-\frac{1.3 \cdot t^2}{T_r^2}\right)\right]. \tag{6}$$

Here, T_d and T_r are decay and rise times, respectively.

The calculations of the pulses presented here start from the Monte Carlo calculated spatial distribution of the energy distribution (history) in the detector volume. The final pulse thus *typically is a sum of a few hundred subpulses* (see Fig. 1) *and it contains all information on the shape and extension of the registered event*.

Table 1
Fit parameters for the experimental drift velocities in the ⟨100⟩ and ⟨111⟩ directions (from [22])

Direction	μ (cm^2/V s)	E_0 (V/cm)	β	μ_n (cm^2/V s)
⟨100⟩	40 180	493	0.72	589
⟨111⟩	42 420	251	0.87	62

Table 2
Main parameters of the enriched Heidelberg–Moscow detectors

Detector	ANG2	ANG3	ANG4	ANG5
Active mass, kg	2.758	2.324	2.295	2.666
Depletion voltage, V	3000	3200	2900	1200
Operational voltage, V	4000	4000	3500	2500
^{76}Ge content, %	86.6	88.3	86.3	85.6
Impurity density, $\times 10^9$ cm^{-3} [18]	(5.36–8.53)	(5.26–9.95)	(4.23–6.49)	(0.233–1.38)
Crystal diameter, mm	80	78.5	75	78.8
Crystal length, mm	108	93.5	100.5	105.7
Bore diameter, mm	8	9	8	8
Bore length, mm	94	81.5	88.9	93.5

3.2. Results of pulse shape calculations

3.2.1. Small events (weighted size $\leqslant 0.5$ mm)

We first consider events of small size. Fig. 4(left) shows pulses for $0\nu\beta\beta$ decay events produced by the λ-term, calculated for events of different sizes (between 0.05 and 0.5 mm (weighted), see Fig. 2) and different radial positions in the detector. Fig. 4(right) shows examples for mass-term and λ-term produced $0\nu\beta\beta$ events together. In Fig. 4 (and also in Fig. 5) the weighted center of energy depositions of the $0\nu\beta\beta$ event in the crystal is set equal to the different radial positions.

One can see that the pulse shapes agree for smaller radii well within this range of sizes. The tiny deviations seen in Fig. 4 for $R = 10$, 20, 30 mm start for weighted (linear) sizes of ~ 0.4 (4) mm. This range of weighted sizes < 0.4 mm includes $\sim 90\%$ of all $0\nu\beta\beta$ events (see Fig. 2, and Fig. 9 in [1]). The same agreement with the other terms, as for the λ and mass term, is found for $0\nu\beta\beta$ events produced by the η-term.

Let us compare two events which are much different in the sizes, according to Monte Carlo simulations. Fig. 5 shows such

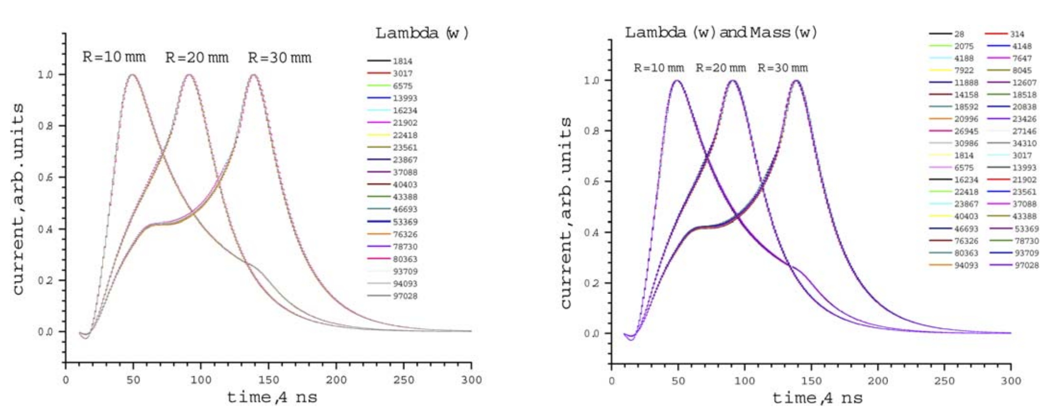

Fig. 4. Left: pulse shapes (20 events) for λ-term calculations—for weighted sizes from ~ 0.05 mm till 0.5 mm in steps equal to ~ 0.05 mm. Right: pulses from the left figure compared with 20 events calculated for mass-term $0\nu\beta\beta$ events (total 40 events, see columns in the figure).

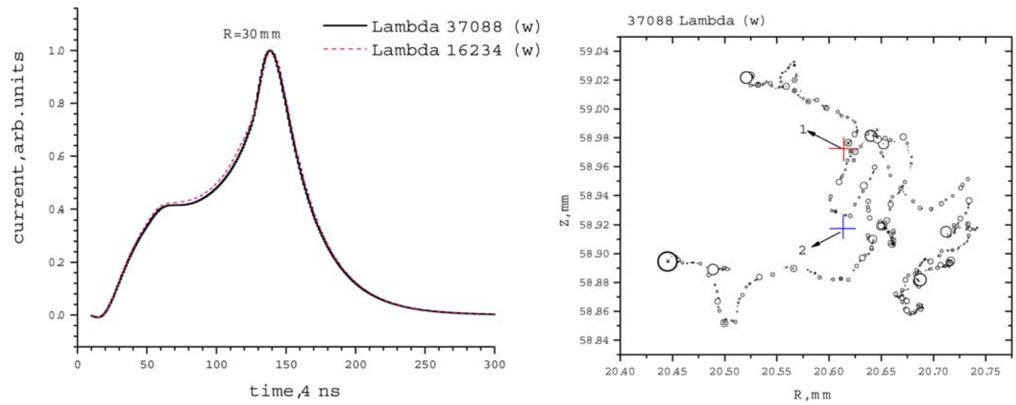

Fig. 5. The comparison of two calculated $0\nu\beta\beta$ events (λ term) with different sizes (event No. 37088 has weighted size (w) 0.07 mm and linear size (l) = 0.33 mm), (see right figure). For event No. 16234 (red dotted line)—$w = 0.5$ mm and $l = 4.65$ mm, see Fig. 6(a). By a red cross (indicated also, as number 1) and a blue cross (indicated as a number 2) are shown the choice of the localization of the event at the different radii of the detector: (2) corresponds to the center of gravity of the event (concerning the energy distribution), (1) starting point of the $\beta\beta$ event.

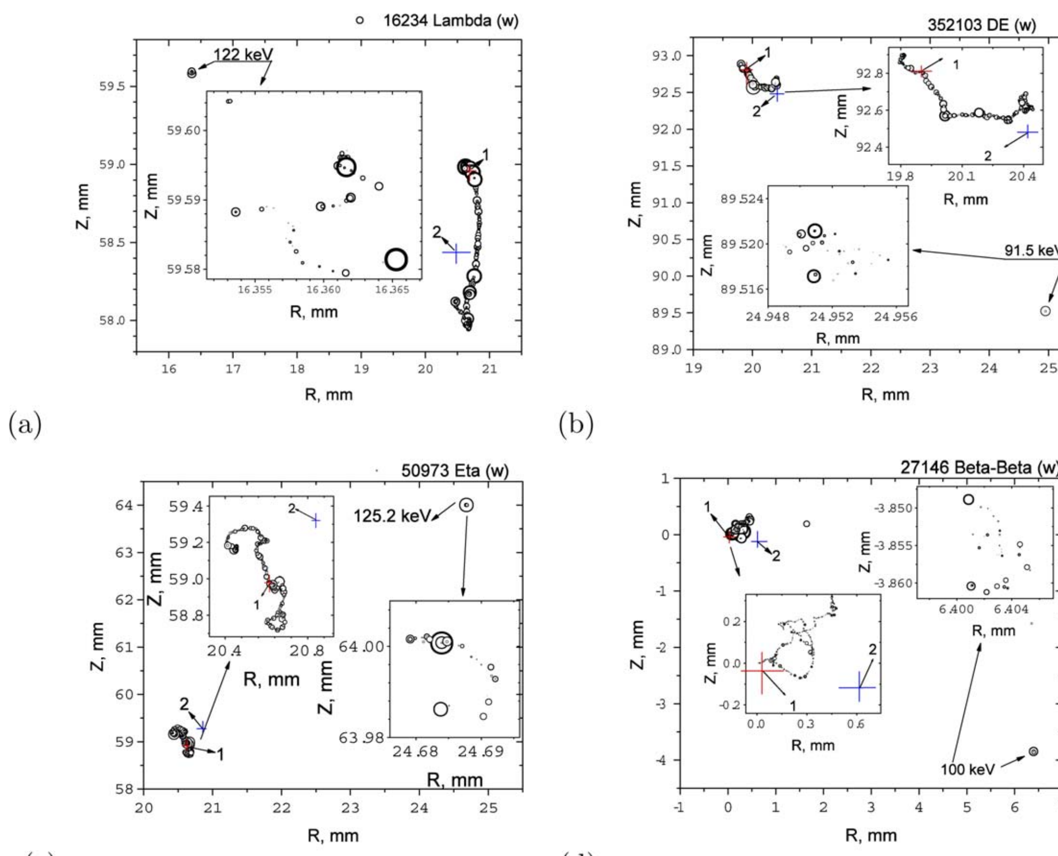

Fig. 6. (a) Track of the $0\nu\beta\beta$ event No. 16234—with size parameters: weighted size $w = 0.5$ mm, linear size $l = 4.65$ mm (λ term calculations), (b) double escape event (DE) No. 352103—with size parameters: $w = 0.5$ mm, $l = 7.09$ mm. (c)—track of $0\nu\beta\beta$ event No. 50973 (from η-term, $w = 0.5$ mm, $l = 6.82$ mm). (d)—track of $0\nu\beta\beta$ event No. 27146 ($w = 0.5$ mm, $l = 7.55$ mm) (from mass-term). In the extra windows the detailed structure of each sub-event is shown. For the description of the red cross (indicated also as number 1) and blue cross (indicated as number 2) see caption of Fig. 5.

example where in some detail the ‘difference’ between two pulses of small (0.07 mm) and larger size (0.5 mm) for λ-term produced events is visible. The structures of these two events are shown in Fig. 5(right) and in Fig. 6(a). One sees almost *no* difference.

At that point we can conclude that:

(1) The Ge detector should allow nicely, by exploiting the shapes of the pulses, to determine the localization of $\beta\beta$ events in radial direction (Fig. 4).

(2) There is for the overwhelming majority of $0\nu\beta\beta$ events *no possibility to differentiate* between *different types* of $0\nu\beta\beta$ events—λ or η or effective mass driven—in a *large vol-*

ume germanium detector. The differences still visible in the theoretical *tracks* (Fig. 2) are *washed out* by the limited position resolution of the detector.

Now, let us compare the *realistic* pulse shape of our Monte Carlo calculated event with a pulse shape calculated with a simplifying approach, in which *all energy* of the event is *deposited in one point (zero range approximation)*. Fig. 7 shows to which extent a already relatively large $0\nu\beta\beta$ event of weighted size of 0.5 mm (linear 4.65 mm, see Fig. 6(a)) can be approximated by such simplified pulse shape calculation.

Let us now go to *another important point* for the $\beta\beta$ experiments and consider events, which we expect from the double escape γ-line. Fig. 8(left) shows calculated pulses (from the microscopic tracks) for the 1592 keV double escape line for sizes between 0.05 and 0.5 mm (weighted). Also here the position of the weighted center of the energy deposition in the detector has been set equal to the radius considered.

Fig. 8(right) shows a comparison of double escape (DE) events and of λ-term $0\nu\beta\beta$ events for sizes between 0.2 and 2.2 mm (linear), step width 0.2 mm, two events for each size (see Table 3). It is visible that in this size range the double escape pulses and $0\nu\beta\beta$ pulses agree very well.

Figs. 9, 10(right) and 11 show similar plots as Fig. 8 but now the *starting* point of the $0\nu\beta\beta$ track (and the position of first interaction of the γ-ray) has been put equal to the radius considered. Although this corresponds to a tiny effective shift of the center of gravity of the energy depositions, the corresponding shift of the radial position is practically *not visible* for events with these sizes.

Fig. 11 shows as further example a *relatively large* $0\nu\beta\beta$ pulse (weighted size 0.5 mm, linear size 6.82 mm) compared with a similar size double escape pulse (size 0.5 (7.09) mm) (see Fig. 6). The very good agreement of the shapes (as in Fig. 8, right) indicates, that looking for shapes of $0\nu\beta\beta$ events with a *neuronal net calibrated to the shapes of the 1592 keV DE γ-line could be helpful*.

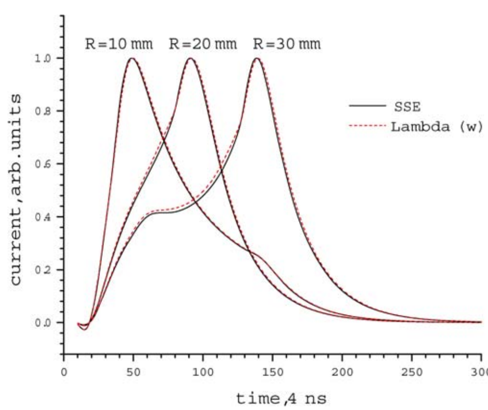

Fig. 7. Comparison of $0\nu\beta\beta$ pulse (No. 16234—see Fig. 6(a)), calculated on the basis of λ-term approach—red (dotted) lines, and a zero range single site event (denoted here by SSE) with a starting point at $R = 10, 20, 30$ mm and $Z = 5.57$ cm (black line) in a big Ge p-type detector.

Table 3
Radii for double escape (DE), and $0\nu\beta\beta$ (λ-term) calculated events, to Fig. 8

Weighted sizes (mm) DE (2614 keV)		Linear sizes (mm)			
		DE (2614 keV)		Lambda (1592 keV)	
Event No.	r_w	Event No.	r_l	Event No.	r_l
42769	0.067	131363	0.342	14359	0.40006
217651	0.079	257890	0.346	47438	0.41032
421745	0.100	258092	0.4049	81232	0.60001
202494	0.100	66478	0.4051	25065	0.60028
52647	0.150	226943	0.6002	5124	0.80004
93437	0.150	148384	0.6009	930	0.80029
187658	0.2	109467	0.8004	7180	1.0
5188	0.2003	418579	0.8004	55067	1.0
442361	0.2501	276814	1.004	4052	1.2
62508	0.25	402658	1.004	5771	1.2
159189	0.301	324070	1.2	9360	1.4
344168	0.302	428763	1.201	14581	1.4
132978	0.357	210070	1.406	44482	1.6
290909	0.361	130746	1.419	90322	1.6
44827	0.401	316105	1.639	57030	1.8001
444801	0.414	448956	1.836	77712	1.8002
156235	0.487	107027	1.859	3888	2.0006
227487	0.450	49526	2.102	14715	2.0006
49526	0.504	224954	2.135	89130	2.2
352103	0.522	76067	2.405	10464	2.2008

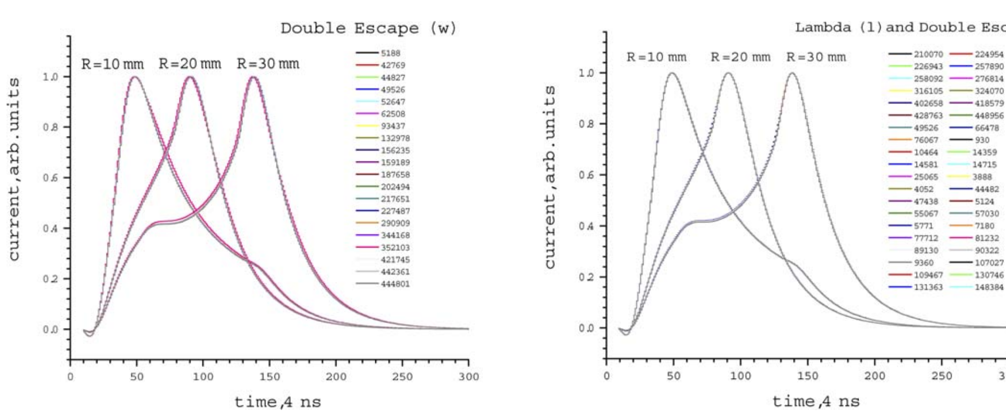

Fig. 8. Left: calculated pulses produced by the double escape (DE) line at 1592 keV of the 2614 keV γ-transition from ^{228}Th for different radii $R = 10, 20, 30$ mm (and $Z = 5.57$ cm), with weighted sizes from 0.05 mm till 0.5 mm with a step equal to ~ 0.05 mm (see Table 3). Right: comparison of 20 $0\nu\beta\beta$ pulses (lambda-term calculations) and 20 pulses produced by the double escape (DE) line at 1592 keV of the 2614 keV γ-transition from ^{228}Th (linear events sizes from 0.2 mm till 2.2 mm in step of 0.2 mm) (see Table 3).

3.2.2. *Events of large sizes ($w > 1$ mm)*

Another *smaller group* of $0\nu\beta\beta$ events was identified from our Monte Carlo calculations as events of large sizes. We shall consider their behaviour in this section. Fig. 12 shows events with weighted sizes between 1 and 4 mm (λ, η and m-type) and also for double escape γ events. The figure shows that for larger sizes ($w > 1$ mm), for individual *events* and *types* the degeneracy in shape *is lifted*. The shapes start to *become different*. The figures show that for large size pulses one can thus expect calibration of pulse shape with a double escape γ line—or with a zero range pulse approximation *to hardly any more lead* to good fits of double beta events. Whether these differences can be explored to get information from such large size events on the type of the event (λ, η and m) has to be investigated in more detail. *It does not look promising* for a (*usually*) low-statistics $\beta\beta$ experiment.

It should be noted that a few of the large pulses shown in Fig. 12, are *not fully contained* any more *in the detector*, which affects of course their pulse shape.

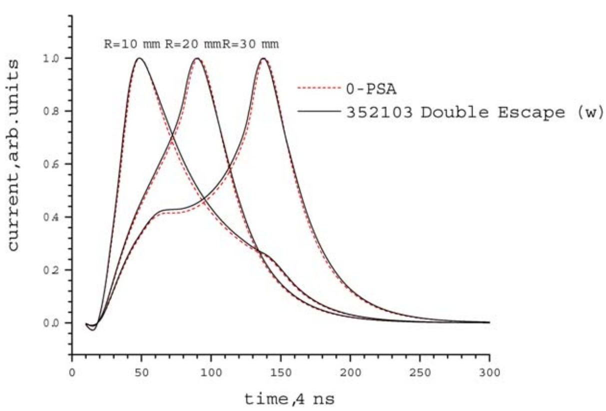

Fig. 9. The pulse No. 352103—(see Fig. 6-right top), produced by the double escape line at 1592 keV of the 2614 keV γ-transition from ^{228}Th with the *starting* point at $R = 10, 20, 30$ mm and $Z = 5.57$ cm (red dotted lines) compared with zero range single site events (SSE) with a starting point at $R = 10, 20, 30$ mm and $Z = 5.57$ cm (black lines).

3.3. *Test of the libraries by source measurements*

For the purpose of test of the calculations of the pulse shapes, for the *first time* extensive measurements of pulse shapes of events from *collimated* γ sources were performed with the detectors of the Heidelberg–Moscow experiment in the period July–September 2004, after the experiment had been stopped in November 2003. These measurements were performed in the Gran Sasso underground laboratory, in the same building, where the Heidelberg–Moscow experiment was located and with the same electronics and data acquisition setups as used for the main experiment 1995–2003 [3–5,10–15].

The energy outputs of the preamplifiers were amplified by two separate amplifiers with different gains. After amplification, the energy of an event was measured by two ADCs and written to the list-mode file. The timing output of the preamplifier was digitized (amplification and differentiation by TFA (timing filter amplifier)) by a flash-ADC with a sampling frequency of 250 MHz. The data were written to a hard-disk in a binary format and analyzed offline by using a separate conversion code. The conversion code transforms data into ASCII format for further analysis and performs the neuronal network discrimination of the pulse shapes as used during the Heidelberg–Moscow experiment.

During the calibration measurements for the pulse shapes, each detector was placed in a separate lead shielding to suppress the background from the surroundings. A lead collimator was used in the runs with a ^{228}Th source (of 1.4 kBq intensity), with an aperture of Ø2 mm and thickness of 100 mm. The position of the collimator with respect to the detectors was defined with an accuracy of better than 0.5 mm. The collimator was placed as close to the detector copper cap as possible. The distance between the end of the collimator and the crystal surface for the top illumination was about 5–10 mm, depending on the detector design. When the collimator was placed below the detector, this distance was about 50–100 mm. Measurements were done in steps of 10 mm in radial direction ($R = 10, 20, 30$ mm) for the irradiation from top and from bottom of the detector and for

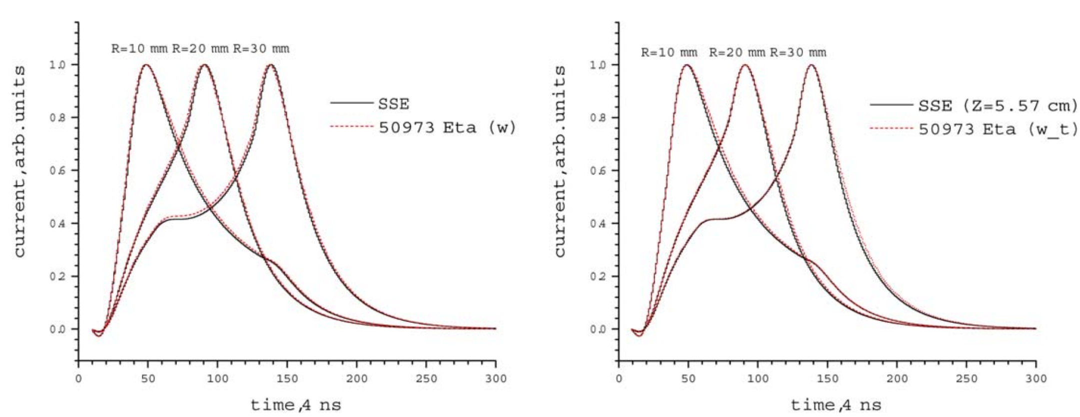

Fig. 10. Left: comparison of $0\nu\beta\beta$ pulse (No. 50973 from η-term calculations—red dotted lines) with zero size (SSE) calculated events (black lines), at $R = 30, 20, 10$ mm and $Z = 5.57$ cm (position of the *center of gravity* of the event set equal to the radius). Right: the same, but now setting the *starting* point of the event equal to the radii.

one or two points in Z direction. For any specific position of the collimator, measurements were done to accumulate a total number of events in the 2614 keV line for the ^{228}Th source up to 10^5, with up to 10^3 events in the 1592 keV double-escape peak. Typical acquisition times for one point were between 3 and 24 hours.

Optimization of the libraries to the level finally achieved in the previous section was done iteratively in order to reach simultaneously the best possible localization of events along the detector volume for a given placement of the collimator, as well as to reach the best suppression of the 1620 keV line which is mainly consisting of higher multiplicity (larger size) events similar to the full energy peak at 2614 keV with respect to the double escape γ-line of the 2614 keV transition, at 1592 keV, which is known to consist of very sharply localized events (see Fig. 2). This optimization was done mostly by slightly varying the density of the ionized impurities inside the detector, and by scaling of the hole mobility.

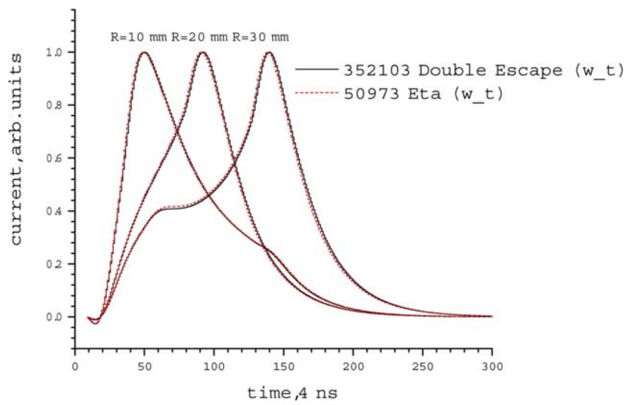

Fig. 11. Comparison of $0\nu\beta\beta$ pulses No. 50973 ($w = 0.5$ mm, linear = 6.82 mm) (see Fig. 6(c)) from η-term calculations—red dotted lines) with pulse No. 352103 (weighted size = 0.5 mm and linear size = 7.09 mm, see Fig. 6(b)) produced by the double escape line at 1592 keV of the 2614 keV γ-transition from ^{228}Th for radii $R = 10, 20, 30$ mm and $Z = 5.57$ cm (black lines). For both pulses the *starting* points of the events have been set equal to the radii.

In Fig. 13, the energy spectrum for the detector ANG5 measured with the ^{228}Th source is shown in the energy interval that covers both the double-escape peak for the most intense 2614 keV line of ^{228}Th source, and the 1620 keV line. Fig. 14 shows an example of the result of the analysis of the source measurements for the 238 keV γ-line from ^{228}Th, positioned at $R = 10$ mm. These low-energy γ-events should be well localized in the detector (SSE events). The radial distribution determined from the analysis of the pulse shapes agrees well with the expectation. The *radial position* resolution is seen to be of the order of a few mm. Fig. 16 shows the corresponding expectation from GEANT4 Monte Carlo calculations (for a radius of 20 mm). Let us now have a look into the spatial resolution of the detectors *in the Z direction* which is demonstrated in Fig. 15 by fit of an event of the spectrum measured in the Heidelberg–Moscow experiment (Run 1067, event No. 41, $E = 2036$ keV). We find a weakness of the position resolution

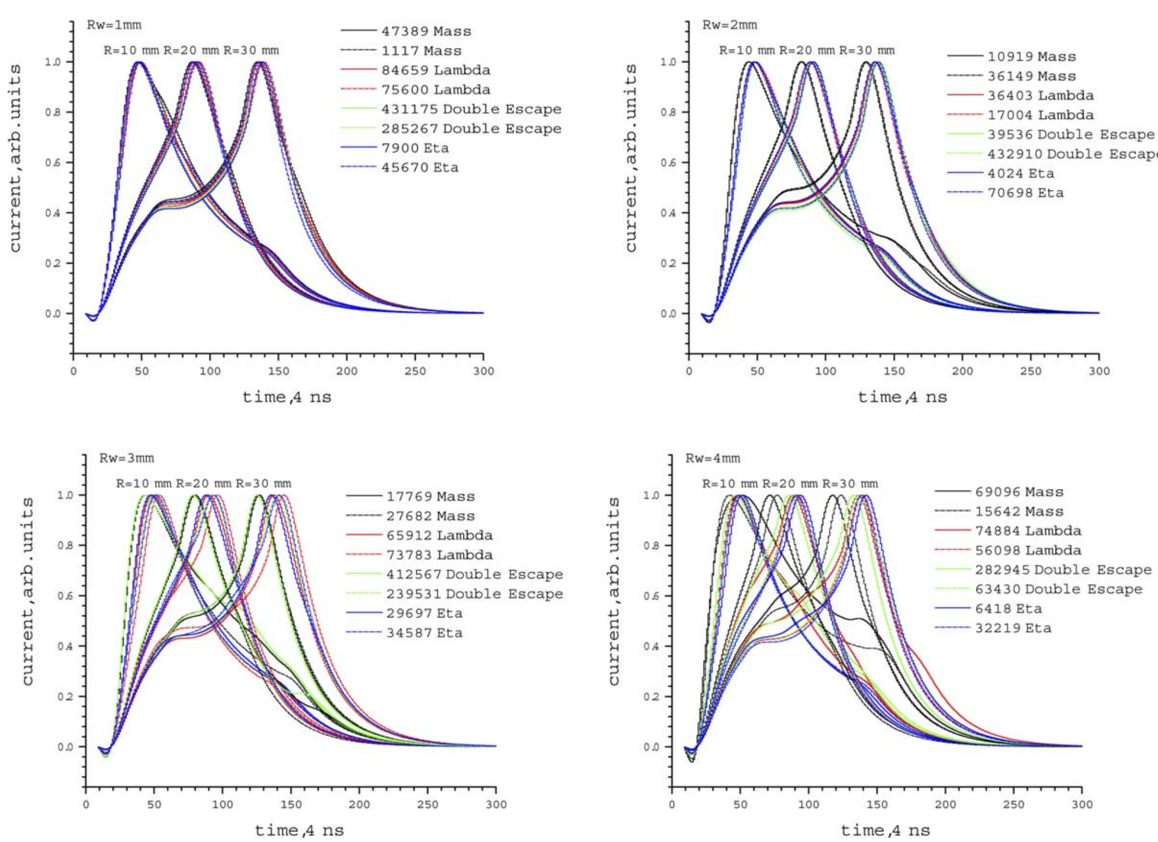

Fig. 12. Calculated pulses for two events for each calculated term (λ, η, m, DE) for weighted sizes 1–4 mm for different radii $R = 10, 20, 30$ mm and $Z = 5.57$ cm.

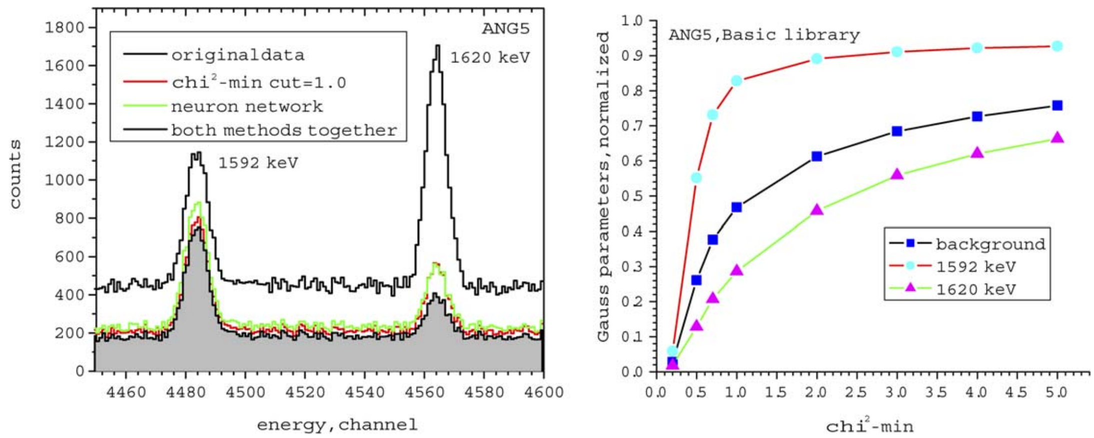

Fig. 13. Left: energy spectrum in the region around the double escape peak of the 2614 keV γ-transition from ^{228}Th for the full data obtained by summing the calibrations with *all used orientations* of the collimator, and for the cut by χ^2-min equal 1.0 for detector 5 (see right figure). The zero-range library accepts about 82% of the double escape peak, while rejecting 72% of the 1620 keV events and 53% of Compton background events. When both methods are used in parallel, i.e., the new method described here, and the neuronal net method [3,4,17], 80% of the double escape peak is kept, with rejection of 82% of the 1620 keV line. Right: the spectrum shown in the left part of this figure has been fitted with Gaussian peaks. The normalized intensities obtained by the fit are plotted as a function of the χ^2-min cut value. We define χ^2 here as a sum of squared deviations between the time structures of measured pulse and library pulse: $\chi^2 = \sum_{n=t05-f}^{t05-l} \frac{(i^n_{\mathrm{exp}} - i^n_{\mathrm{lib}})}{w5} \times 10^3$. Here i^n_{exp} and i^n_{lib} are the (normalized) experimental and library currents for the (time) channel n (one time step is 4 ns per channel of the flash-ADC sampling frequency of 250 MHz). $w5$ is the width at the 5% level of the amplitude (see Fig. 17). χ^2-min gives the degree of agreement of a measured pulse with the library pulse 'closest' in shape (time structure) to the measured pulse. For a detailed description see [39].

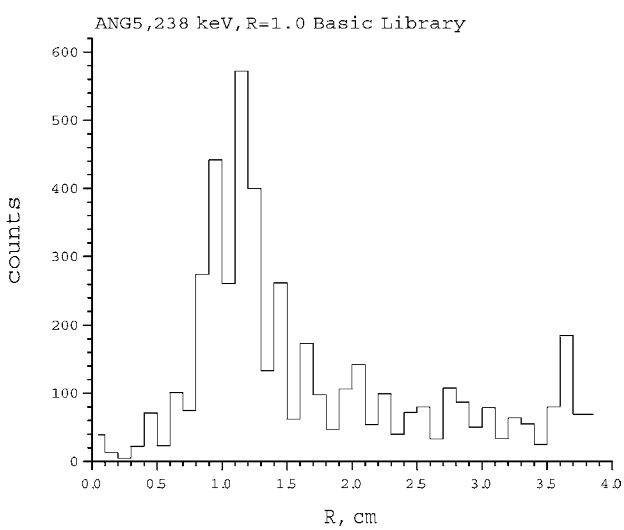

Fig. 14. Radial localization of events of the 238 keV line determined by pulse shape analysis using the zero range library (see text), from measurement with a collimated source.

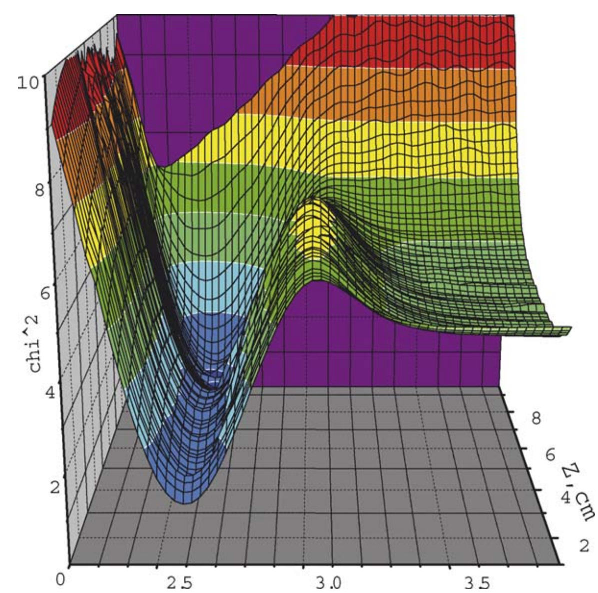

Fig. 15. Fit of the location for an event from the Heidelberg–Moscow $\beta\beta$ measurement seen in the Det. 5, (event No. 41 from the Run 1067, energy—2036 keV) from the measured pulse shape. The weakness in the localization in the Z-direction is obvious and known for Ge detectors (see also [22–25]). Note the offset of the abscissa, which starts at 2.1 cm.

in the Z direction which is a known fact for big coaxial Ge detectors (see, e.g., [22–25]).

4. Application of the calculated pulse shapes to the data of the Heidelberg–Moscow experiment

In this section we briefly show an application of the calculated pulses (zero range approximation), described in Section 3, to pulses of the 1592 keV double escape line of the 2614 keV ^{228}Th line measured with a source, and some of the pulses in the energy range 2036–2042 keV around the measured signal at $Q_{\beta\beta}$ in the Heidelberg–Moscow data set recorded from 1995–2003 with detectors 2, 3, 4 and 5 [3–5,10–15].

Fig. 17 shows that the library described in Section 3 allows to separate single site events from multiple site events. Fig. 18 (left column) shows that pulses *rejected by the neuronal net* [3,4,17] and identified as (multiple site) events, also *cannot be*

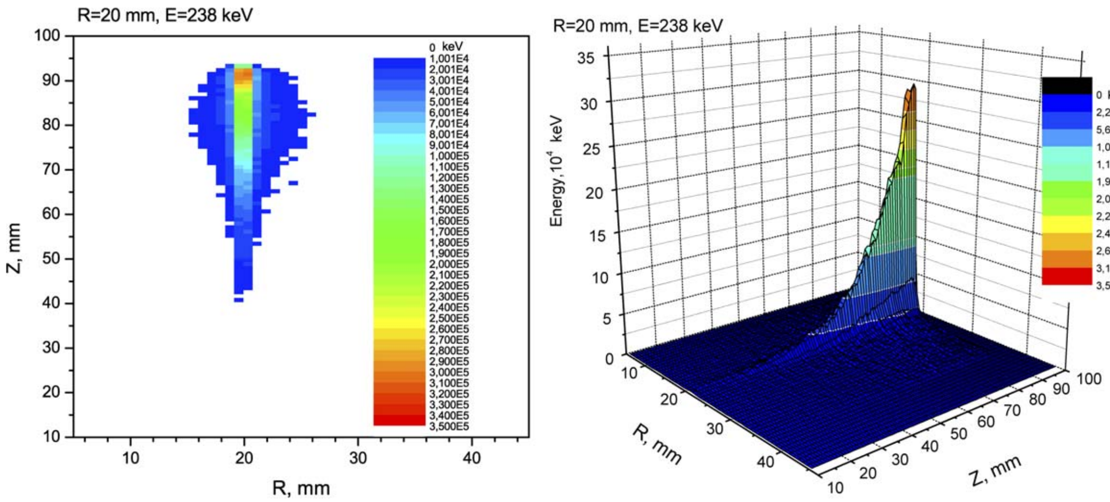

Fig. 16. Spatial distribution of the deposited energy of gamma events, determined by GEANT calculations with a collimated source at the top of the detector at $R = 20$ mm, primary energy of γ-rays 238-keV (height of the detector is 93 mm).

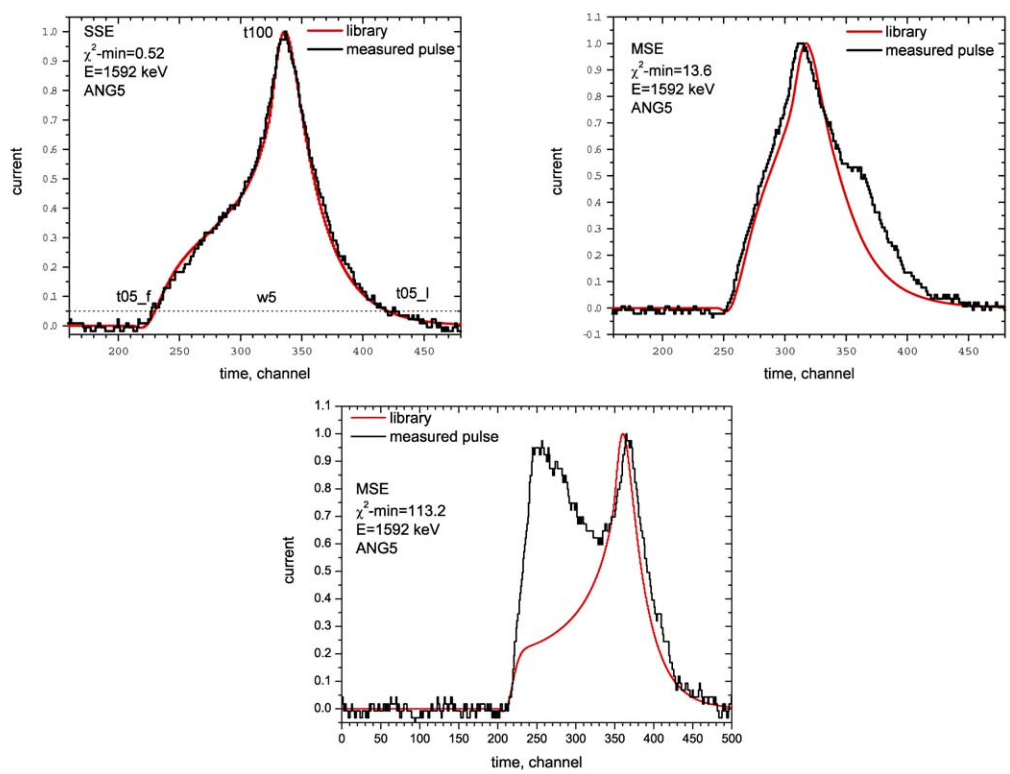

Fig. 17. Result of fitting experimental pulse shapes (black) with the library shapes (red lines) for events of the 1592 keV double escape line of the 2614 keV transition from ^{228}Th. The left (upper) plot represents a single site event (SSE), the right (upper) one a multiple site event (MSE) event. A more drastic MSE event is shown at the bottom.

well fitted by the calculated pulse shape library, developed and described in this Letter.

Thus, comparison with the calculated pulse shapes *also excludes* pulses which cannot originate from a $\beta\beta$ process. So, comparison with calculated pulses can reject the background from multiple site gamma events in the range for $0\nu\beta\beta$ search around $Q_{\beta\beta}$. In the examples (see Fig. 18 (right column)) *accepted by the neuronal net* as single site events, we obtain a *good fit* (small χ^2) with the calculated pulse shapes. A detailed discussion will be given in a separate paper.

5. Conclusions

The identification of signals of neutrinoless double beta decay in a ^{76}Ge detector is a question of extraordinary importance and has therefore found much attention (see, e.g., [16,17,38]). From the time history and spatial energy distribution in a Ge detector of neutrinoless double beta events calculated by a Monte Carlo procedure, we have calculated 'microscopically' for the first time the expected *pulse shapes* to be observed in a germanium detector. The calculated pulses thus consist of a sum of

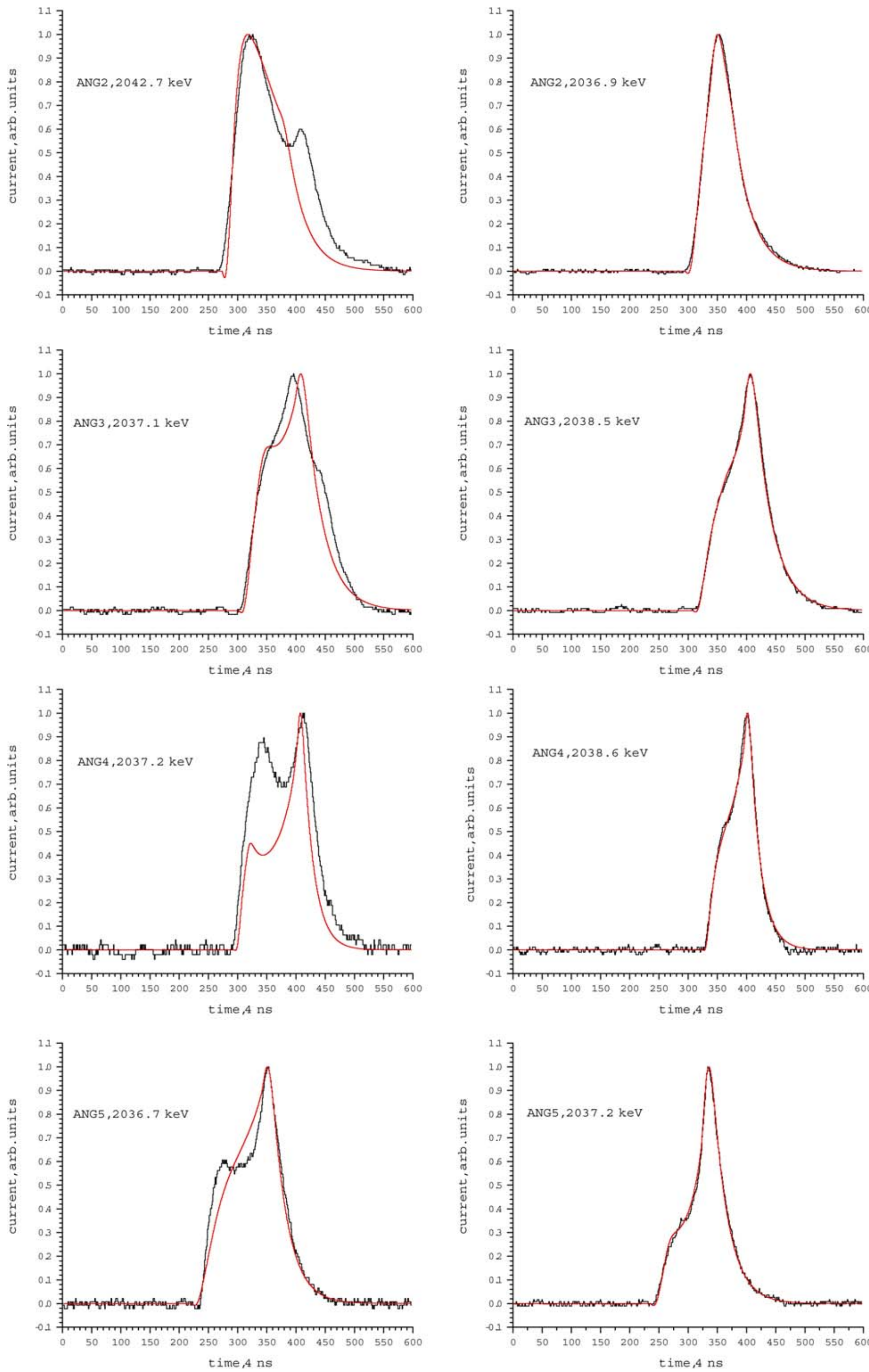

Fig. 18. Time structure *of some* events (black) measured in the Heidelberg–Moscow experiment in the energy region 2036–2042 keV by the four enriched ^{76}Ge detectors (ANG2, ANG3, ANG4, ANG5), which were running with pulse shape analysis (see Fig. 19 in [4]). In the left column of the figure events are shown which were identified, by the neuronal net [3,4] as multiple site events. In the right column of the figure events are shown, identified by *neuronal net* [3,4] as single site events. The red lines show fits of the events *by the zero range* pulse shape approximation library, described in this Letter. The result is consistent with the former neuronal net analysis. The determined χ^2 (for definition see caption of Fig. 13) for the events of the left column are large (21.71, 9.33, 50.03, 6.4). I.e. they are not accepted as SSE. For the events shown in the right column, accepted by the neuronal net as SSE, we find from the pulse shape analysis for χ^2 values $\leqslant 0.5$.

typically several hundred 'sub'-pulses. We show that with the spatial resolution of a large Ge detector there is for the majority of $0\nu\beta\beta$ events ($\geqslant 90\%$), *no chance to differentiate* between the contributions of *different particle physics parameters* entering into the $0\nu\beta\beta$ decay process—in the mass mechanism the effective neutrino mass and the right-handed weak current parameters λ, η. Only for the relatively few $0\nu\beta\beta$ events with *large sizes* one may in principle obtain some information on these basic particle physics parameters. We have further shown, that by *separating small size pulses*, in a ^{76}Ge experiment it is *possible to select* candidats of $0\nu\beta\beta$ events *from background* gamma events. We find that the shapes of theoretically calculated events agree very well with those of measured events near $Q_{\beta\beta}$.

We have also calculated, starting from Monte Carlo simulated spatial energy distributions, pulse shapes for events of the double escape gamma line at 1592 keV of the 2614 keV transition from ^{228}Th. It is shown that the 1592 keV double escape line deliver pulses in the Ge detector *coinciding* to a *large extent* in shape with pulses from neutrinoless double beta decay. *This is of practical importance.* The double escape pulses can be used to build a pulse shape library for search of $0\nu\beta\beta$ decay. We thus have *microscopically shown*, that the *method* used earlier [3–5], (see also [10–14]) namely searching for events of neutrinoless double beta decay by calibrating a neuronal net with the shapes of the 1592 keV double escape line events, has some reliable basis. One can, however, of course not expect that γ-lines in the spectra will be *completely* reduced in a straightforward application of a library produced from such calibration [4,39].

Acknowledgements

We acknowledge the invaluable support from DFG, and LNGS for this project.

References

[1] H.V. Klapdor-Kleingrothaus, I.V. Krivosheina, I.V. Titkova, Phys. Lett. B 632 (2006) 623.
[2] H.V. Klapdor-Kleingrothaus, I.V. Krivosheina, I.V. Titkova, Phys. Rev. D 73 (2006) 013010;
H.V. Klapdor-Kleingrothaus, I.V. Krivosheina, I.V. Titkova, Int. J. Mod. Phys. A 21 (6) (2006) 1159.
[3] H.V. Klapdor-Kleingrothaus, I.V. Krivosheina, A. Dietz, et al., Phys. Lett. B 586 (2004) 198.
[4] H.V. Klapdor-Kleingrothaus, A. Dietz, I.V. Krivosheina, et al., Nucl. Instrum. Methods A 522 (2004) 371.
[5] H.V. Klapdor-Kleingrothaus, et al., Mod. Phys. Lett. A 16 (2001) 2409;
H.V. Klapdor-Kleingrothaus, et al., Found. Phys. 31 (2002) 1181;
H.V. Klapdor-Kleingrothaus, et al., Found. Phys. 33 (2003) 679, Erratum.
[6] G. Douysset, et al., Phys. Rev. Lett. 86 (2001) 4259.
[7] J.G. Hykawy, et al., Phys. Rev. Lett. 67 (1991) 1708.
[8] G. Audi, A.H. Wapstra, Nucl. Phys. A 595 (1995) 409.
[9] R.J. Ellis, et al., Nucl. Phys. A 435 (1985) 34.
[10] H.V. Klapdor-Kleingrothaus, in: R. Shrock (Ed.), Proc. of International Conf. Neutrinos and Implications for Physics Beyond the Standard Model, Stony Brook, USA, 11–13 October 2002, World Scientific, Singapore, 2003, pp. 367–382;
H.V. Klapdor-Kleingrothaus, in: H.V. Klapdor-Kleingrothaus (Ed.), Proc. of International Conf. Beyond the Desert 2003, BEYOND03, Tegernsee, Germany, 9–14 June, 2003, Springer, Heidelberg, 2004, pp. 307–364.
[11] H.V. Klapdor-Kleingrothaus, Nucl. Phys. B (Proc. Suppl.) 143 (2005) 229, in: Proc. of International Conf. Neutrino 2004, Paris, France, 14–19 June 2004.
[12] H.V. Klapdor-Kleingrothaus, Nucl. Phys. B (Proc. Suppl.) 145 (2005) 219, in: G. Fogli, et al. (Eds.), Proc. of International Workshop Neutrino Oscillation, NOW 2004, Bari, Italy, 11–17 September, 2004.
[13] H.V. Klapdor-Kleingrothaus, hep-ph/0512263, in: M. Baldo-Ceolin, (Ed.), Proc. of International Conf. Neutrino Telescopes, February 2005, p. 215.
[14] H.V. Klapdor-Kleingrothaus, Int. J. Mod. Phys. D 13 (2004) 2107.
[15] H.V. Klapdor, Proposal, MPI-1987-V17, September 1987.
[16] J. Hellmig, H.V. Klapdor-Kleingrothaus, Nucl. Instrum. Methods A 455 (2000) 638.
[17] B. Majorovits, H.V. Klapdor-Kleingrothaus, Eur. Phys. J. A 6 (1999) 463.
[18] ORTEC company, T. Raudorf, private communication, 2006.
[19] L. Reggiani, C. Canali, F. Nava, G. Ottaviani, Phys. Rev. B 16 (1977) 2781.
[20] http://laacg1.lanl.gov/laacg/.
[21] K. Siegbahn, Alpha-, Beta- and Gamma-Ray Spectroscopy, vols. 1, 2, fourth ed., North-Holland, Amsterdam, 1974;
G.F. Knoll, Radiation Detection and Measurement, second ed., Wiley, New York, 1989.
[22] L. Mihailescu, W. Gast, et al., Nucl. Instrum. Methods A 447 (2000) 350.
[23] K. Vetter, et al., Nucl. Instrum. Methods A 452 (2000) 105.
[24] K. Vetter, et al., Nucl. Instrum. Methods A 452 (2000) 223.
[25] Th. Kröll, D. Bazzacco, Nucl. Instrum. Methods A 463 (2001) 227.
[26] S. Ramo, Proc. IRE 27 (1939) 584.
[27] W. Shockley, J. Appl. Phys. 9 (1938) 635.
[28] G. Cavalleri, et al., Nucl. Instrum. Methods 21 (1963) 177.
[29] C.E. Lehner et al., in: Proc. of Electronics Engineers Nucl. Science Symp., San Diego, CA, 5–10 November 2001, preprint: UCRL-JC-143745.
[30] Origin (Scientific Graphing & Analysis Software), vers. 7.5, http://www.OriginLab.com.
[31] GEANT4 Collaboration, http://geant4.web.cern.ch/geant4/.
[32] M. Doi, T. Kotani, et al., Prog. Theor. Phys. 67 (1982) 281.
[33] M. Doi, T. Kotani, H. Nishiura, E. Takasugi, Prog. Theor. Phys. 70 (1983) 1353.
[34] M. Doi, T. Kotani, E. Takasugi, Prog. Theor. Phys. Suppl. 83 (1985) 1.
[35] M. Doi, T. Kotani, E. Takasugi, Phys. Rev. C 37 (1988) 2104.
[36] K. Muto, H.V. Klapdor, in: H.V. Klapdor (Ed.), Neutrinos, Graduate Texts in Contemporary Physics, Springer, Berlin, 1988, pp. 183–238.
[37] K. Muto, E. Bender, H.V. Klapdor, Z. Phys. A: At. Nucl. 334 (1989) 187;
K. Muto, E. Bender, H.V. Klapdor, Z. Phys. A: At. Nucl. 334 (1989) 177.
[38] D. Gonzáles, et al., Nucl. Instrum. Methods A 515 (2003) 634.
[39] H.V. Klapdor-Kleingrothaus, et al., to be published.